IEEE Access
Multidisciplinary ⋮ Rapid Review ⋮ Open Access Journal

Received May 25, 2020, accepted June 14, 2020, date of publication June 19, 2020, date of current version July 8, 2020.

Digital Object Identifier 10.1109/ACCESS.2020.3003681

Distributed Adaptive Fault-Tolerant Control for Spacecraft Formation With Communication Delays

PENG LI[1], ZONGMING LIU[2], CHENYU HE[1], QI LIU[1], AND XIAO-QING LIU[3]

[1]School of Automation and Electronic Information, Xiangtan University, Xiangtan 411105, China
[2]Shanghai Institute of Spaceflight Control Technology, Shanghai 201109, China
[3]Department of Precision Instrument, Tsinghua University, Beijing 100084, China

Corresponding author: Xiao-Qing Liu (lxq17@mails.tsinghua.edu.cn)

This work was supported in part by the National Project Funding for Key Research and Development Programs under Grant 2018YFC0808500, and in part by the Keypoint Research and Invention Program of Hunan Province, China, under Grant 2018GK2014.

ABSTRACT This paper investigates distributed adaptive fault-tolerant control schemes for spacecraft formation subject to external disturbances, model uncertainties and communication delays. Two novel adaptive fault-tolerant control approaches are presented based on directed communication interaction. The developed adaptive laws are used to estimate the actuator effectiveness, the spacecraft masses and the upper bound on external disturbances. Then, an adaptive fault-tolerant control algorithm with time-varying communication delays is proposed. In particular, the conditions on the controller parameters and the communication delays necessary to assure the asymptotic stability of the closed-loop system are given. Finally, numerical simulations are presented to validate the effectiveness of the two proposed fault-tolerant control schemes for the spacecraft formation system.

INDEX TERMS Spacecraft formation, fault-tolerant control, communication delays, actuator fault, asymptotic stability.

I. INTRODUCTION

During the past decade, spacecraft formation flying (SFF), which is a scenario involving two or more spacecraft maneuvering in a tightly controlled spatial configuration, has been intensively investigated. SFF shows great potential for various space missions, such as distributed aperture radar, Earth stereo-imaging and deep-space observation [1]–[3]. To accomplish these missions, the relative positions of the spacecraft within the formation should be maintained with a high accuracy. From a practical point of view, the design of an efficient coordinated control approach for relative position maintenance in SFF is undoubtedly a central issue related to trajectory tracking during maneuver. Due to the characteristics of SFF, the coordinated control of the relative positions of spacecraft has attracted increasing attention recently.

Various distributed control algorithms have been presented for SFF on the basis of local information interaction [4]–[8]. Generally, the control approaches for SFF can be divided into three main categories, namely, behavioral-based formation control, leader-follower formation control, and virtual-structure-based formation control [2]. Correspondingly, various formation control algorithms for SFF have been investigated. For instance, Zhang *et al.* present three different coordinated controllers for SFF using hyperbolic tangent functions and behavior-based control [4]. Based on the leader-follower approach, Subbarao, *et al.* propose a novel nonlinear control approach for multiple free-flying spacecraft such that the relative position vector between a pursuer and a target spacecraft will always be directed toward the docking port of the target [5]. In [6], several approaches for the tracking control of the relative motion of spacecraft in a leader–follower formation are derived, and the control performances of the proposed controllers are studied. Ran *et al.* address a coordinated control problem for relative positions in SFF using a directed communication topology, in which time-varying and bounded communication delays are also considered [7]. Hu *et al.* develop a finite-time coordinated relative position tracking controller without velocity information, for which the Lyapunov stability of the closed-loop system is given [8].

The associate editor coordinating the review of this manuscript and approving it for publication was Zhong Wu.

Although most of the existing control algorithms for SFF are elegant and intuitively appealing, they require the implicit assumptions that the actuator is healthy and that no the actuator faults emerge. In fact, the fault tolerance capacity of control algorithms is a fundamental issue in SFF systems [9]. Consequently, it is essential to design formation control algorithms subject to actuator fault constraints. Hence, many fault-tolerant control approaches have been addressed in recent decades. Wang *et al.* propose an adaptive fault-tolerant control approach to solve the problems of actuator faults and time delays for uncertain switched nonaffine nonlinear systems [10]. Wu *et al.* present a cooperative observer-based fault-tolerant control approach based on the time-varying asymmetric network structure [11]. However, it is difficult to apply the control methods introduced in [10], [11] for fault-tolerant SFF control because of the strong nonlinearity of the spacecraft model. In [12], [13], adaptive fault-tolerant sliding mode control strategies are proposed to control a formation of unmanned aerial vehicles. In [14], distributed adaptive fault-tolerant coordinated attitude control laws are proposed for the case in which the reference signal is available only to a subset of the spacecraft. In [15], distributed adaptive formation control algorithms for unmanned aerial vehicles in the presence of input saturation, external disturbances and actuator faults are addressed. However, it should be noted that to the best knowledge of the authors, coordinated control schemes for multiple spacecraft with actuator faults and model uncertainty have seldom been considered. In addition, communication delays have not been considered in most of the literature.

In this study, distributed adaptive fault-tolerant control schemes for SFF are proposed to address problems of relative position control during maneuvers. Moreover, time-varying communication time delays are considered in the stability analysis. Compared with previous works, this paper offers three main contributions. First, a novel fault-tolerant control approach for SFF is established to simultaneously address the problems of actuator faults, external disturbances and parameter uncertainties. In contrast to active fault-tolerant control, the proposed control algorithms do not require fault diagnosis. Second, the presented adaptive laws are designed to estimate unknown parameters, such as the spacecraft masses, the actuator effectiveness and the upper bound on disturbances. The stability of the closed-loop system is also strictly addressed using the Lyapunov method. Last but not least, time-varying communication time delays are considered, in contrast to the existing work on constant delays in [16]–[18].

The remainder of this paper is organized as follows. The related fundamental theory, including the SFF model, the formulation of the positions of the spacecraft within a formation and basic graph theory, is introduced in Section II. Subsenquently, a distributed fault-tolerant adaptive control algorithm for SFF with external disturbances and parameter uncertainties is proposed in Section III. Then, a distributed fault-tolerant adaptive control algorithm with communication delays is presented to simultaneously address time-varying communication delays, external disturbances and actuator faults. A corresponding stability analysis is also strictly derived. Numerical simulation results are presented in Section IV, and Section V concludes the paper.

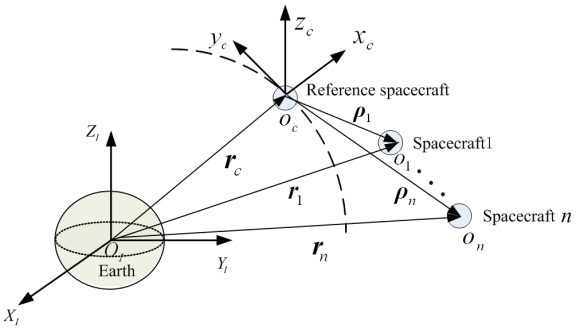

FIGURE 1. Schematic representation of SFF.

II. RELATED FUNDAMENTAL THEORY

A. MATHEMATICAL MODEL

In this section, a nonlinear relative motion model for SFF is introduced. Suppose that there exists a virtual reference spacecraft flying in an ideal elliptical orbit, and that another n spacecraft moving in a desired formation configuration, as presented in Fig. 1. r_c is the radial distance from the center of the Earth to the virtual spacecraft. In addition, a local-vertical-local-horizontal (LVLH) frame with its origin at the center of the virtual spacecraft is introduced, where the x_c axis points along the radial direction, the y_c axis points along the direction normal to the orbital plane, and the z_c axis is the third axis of the right-handed frame.

In the LVLH frame, the relative position and relative velocity of the ith spacecraft with respect to the reference spacecraft are denoted by $\boldsymbol{\rho}_i$ and $\boldsymbol{v}_i$, respectively. The nonlinear relative motion model for the ith spacecraft in the LVLH frame can be described by [6]

$$\begin{aligned}\dot{\boldsymbol{\rho}}_i &= \boldsymbol{v}_i \\ m_i\dot{\boldsymbol{v}}_i &= \boldsymbol{C}_i(\dot{\theta}_c)\boldsymbol{v}_i + \boldsymbol{D}_i(\ddot{\theta}_c,\ \dot{\theta}_c,\ r_i)\boldsymbol{\rho}_i + \boldsymbol{n}_i(r_i,\ r_c) + \boldsymbol{h}_i + \boldsymbol{F}_i\end{aligned} \tag{1}$$

where

$$\boldsymbol{C}_i(\dot{\theta}_c) = 2m_i\dot{\theta}_c\begin{bmatrix} 0 & 1 & 0 \\ -1 & 0 & 0 \\ 0 & 0 & 0 \end{bmatrix} \tag{2}$$

$$\boldsymbol{D}_i(\ddot{\theta}_c,\ \dot{\theta}_c,\ r_i) = -m_i\frac{\mu}{r_i^3}\boldsymbol{I} + m_i\begin{bmatrix} \dot{\theta}_c^2 & \ddot{\theta}_c & 0 \\ -\ddot{\theta}_c & \dot{\theta}_c^2 & 0 \\ 0 & 0 & 0 \end{bmatrix} \tag{3}$$

$$\boldsymbol{n}_i(r_i,\ r_c) = \mu m_i[-\frac{r_c}{r_i^3} + \frac{1}{r_c^2} \quad 0 \quad 0]^{\mathrm{T}} \tag{4}$$

m_i is the mass of the ith spacecraft, $\boldsymbol{h}_i$ is a bounded disturbance force such that $\|\boldsymbol{h}_i\|_\infty \leq d_{i1}$, $\boldsymbol{F}_i$ is the control input acting on the ith spacecraft, θ_c is the true anomaly of the reference spacecraft, r_i represents the distance between

the reference spacecraft and the ith spacecraft, and μ is the gravitational constant of the Earth.

In this study, multiplicative and additive actuator faults are considered, which are formulated as

$$\boldsymbol{F}_i = \boldsymbol{\Gamma}_i \boldsymbol{f}_i + \boldsymbol{\delta}_i \tag{5}$$

where $\boldsymbol{f}_i$ is the signal generated by the controllers to be designed, $\boldsymbol{\Gamma}_i = \text{diag}\{\alpha_{i1}, \alpha_{i2}, \alpha_{i3}\}$ is a time-varying diagonal matrix, and $\boldsymbol{\delta}_i$ represents additive faults in the control input channels. It can be seen that the case of $\alpha_{ij} = 1$ $(j = 1, 2, 3)$ means that the jth actuator of the ith spacecraft is free from multiplicative actuator faults, whereas $\alpha_{ij} < 1$ indicates that the jth actuator has partially lost its effectiveness, but can still function all times.

Assumption 1: The components of $\boldsymbol{\Gamma}_i$ satisfy $0 < \underline{\alpha}_i \leq \min\{\alpha_{i1}, \alpha_{i2}, \alpha_{i3}\} \leq 1$, where $\underline{\alpha}_i$ is an unknown constant. In addition, $\boldsymbol{\delta}_i$ is bounded such that $\|\boldsymbol{\delta}_i\|_\infty \leq d_{i2}$.

The objective in this paper is to design a distributed fault-tolerant formation controller such that all spacecraft can maintain the designed formation configuration. Moreover, the spacecraft follows a prescribed reference trajectory.

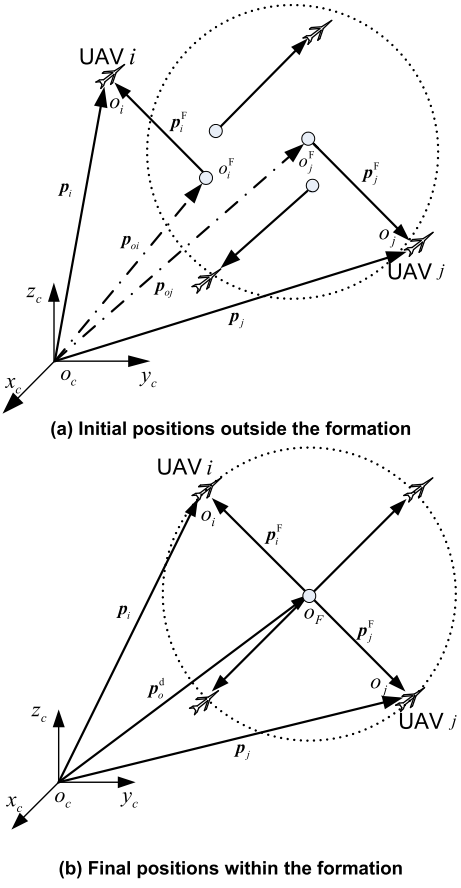

(a) Initial positions outside the formation

(b) Final positions within the formation

FIGURE 2. Schematic representation of formation keeping.

B. POSITIONS WITHIN THE FORMATION

Formation coordination requires the spacecraft to maintain their geometric configuration during formation maneuvers. In this study, the desired position of the ith spacecraft is expressed as $\boldsymbol{\rho}_i^{\mathrm{d}} = \boldsymbol{\rho}_o^{\mathrm{d}} + \boldsymbol{\rho}_i^{\mathrm{F}}$, where $\boldsymbol{\rho}_o^{\mathrm{d}}$ is the desired center position of the formation, and $\boldsymbol{\rho}_i^{\mathrm{F}}$ is the desired position of the ith spacecraft relative to this center position. In Fig. 2 (a), the spacecraft do not form the desired configuration at the initial time. o_i^{F} is the virtual center of the formation determined from the ith spacecraft through the relation $\boldsymbol{\rho}_o^i = \boldsymbol{\rho}_i^{\mathrm{d}} - \boldsymbol{\rho}_i^{\mathrm{F}}$. In fig. 2 (b), the desired configuration is realized. Here, the virtual formation center o_i^{F} of the ith spacecraft overlaps with the virtual formation centers of all the other spacecraft at the common formation center o_F. Indeed, the desired configuration is realized if and only if all of the virtual formation centers o_i^{F} overlap $(\boldsymbol{\rho}_o^i = \boldsymbol{\rho}_i - \boldsymbol{\rho}_i^{\mathrm{F}} \to \boldsymbol{\rho}_j - \boldsymbol{\rho}_j^{\mathrm{F}} = \boldsymbol{\rho}_o^j)$. Our aim is to design control algorithms to track the desired trajectories such that $\boldsymbol{\rho}_i \to \boldsymbol{\rho}_i^{\mathrm{d}}$ and $\boldsymbol{v}_i \to \boldsymbol{v}_i^{\mathrm{d}}$ as $t \to \infty$. Note that $\boldsymbol{\rho}_i \to \boldsymbol{\rho}_i^{\mathrm{d}}$ and $\boldsymbol{v}_i \to \boldsymbol{v}_i^{\mathrm{d}}$ represents the realization of station keeping, and that $\boldsymbol{\rho}_i - \boldsymbol{\rho}_i^{\mathrm{F}} \to \boldsymbol{\rho}_j - \boldsymbol{\rho}_j^{\mathrm{F}}$ represents that formation keeping is achieved during transition.

C. BASIC GRAPH THEORY

In this paper, a graph theory framework is introduced to analyze and synthesize the proposed control scheme for SFF. A weighted directed graph $\mathrm{G} = (\nu, \varsigma, \boldsymbol{C})$ consists of a node set $\nu = \{1, 2 \ldots, n\}$, an edge set $\varsigma \subseteq \nu \times \nu$, and a weighted adjacency matrix $\boldsymbol{C}$. If there exists information interaction from the jth node to the ith node, then there is an edge from the jth node to the ith node, denoted by $(i, j) \in \varsigma$. An element of the adjacency matrix $\boldsymbol{C}$ takes a value of $c_{ij} > 0$ if $(i, j) \in \varsigma$ and $i \neq j$, otherwise $c_{ij} = 0$. The directed graph is called balanced if and only if $\sum_{j=1}^{n} a_{ij} = \sum_{j=1}^{n} a_{ji}$ for $i = 1, \cdots n$.

III. MAIN RESULTS

A. DISTRIBUTED FAULT-TOLERANT CONTROLLER

In this section, it is assumed that the masses of the spacecraft are unavailable due to fuel consumption or measurement uncertainty. The position and velocity tracking errors of the ith spacecraft are defined as $\boldsymbol{e}_{i1} = \boldsymbol{\rho}_i - \boldsymbol{\rho}_i^{\mathrm{d}}$ and $\boldsymbol{e}_{i2} = \boldsymbol{v}_i - \boldsymbol{v}_i^{\mathrm{d}}$, respectively. Consequently, a composite error variable can be defined as

$$\boldsymbol{s}_i = \boldsymbol{e}_{i2} + k_i \boldsymbol{e}_{i1} \tag{6}$$

From Eqs. (1), (5) and (6), it follows that

$$m_i \dot{\boldsymbol{s}}_i = m_i \boldsymbol{Y}_i + \boldsymbol{d}_i + \boldsymbol{\Gamma}_i \boldsymbol{f}_i \tag{7}$$

where $\boldsymbol{d}_i = \boldsymbol{h}_i + \boldsymbol{\delta}_i$, and

$$\boldsymbol{Y}_i = \frac{1}{m_i}\left[\boldsymbol{C}_i(\dot{\theta}_c)\boldsymbol{v}_i + \boldsymbol{D}_i(\ddot{\theta}_c,\ \dot{\theta}_c,\ r_i)\boldsymbol{\rho}_i + \boldsymbol{n}_i(r_i,\ r_c)\right] + k_i(\boldsymbol{v}_i - \boldsymbol{v}_i^{\mathrm{d}}) - \dot{\boldsymbol{v}}_i^{\mathrm{d}} \tag{8}$$

The total disturbance $\boldsymbol{d}_i$ is bounded such that

$$\|\boldsymbol{d}_i\|_\infty \leq \|\boldsymbol{h}_i\|_\infty + \|\boldsymbol{\delta}_i\|_\infty \leq d_{i1} + d_{i2} = \bar{d}_i \tag{9}$$

where $\bar{d}_i$ is the upper bound on the total disturbance. Accordingly, the following lemmas are presented.

Lemma 1: Let $\sigma_i(t) > 0$ be a bounded function, and let x be a scalar; then, the following relationship holds:

$$0 \le |x| - \frac{x^2}{\sqrt{x^2 + \sigma_i^2(t)}} < \sigma_i(t) \tag{10}$$

Furthermore, there exists a function $\sigma_i(t)$, such that

$$\lim_{t\to\infty} \int_0^t \sigma_i(\tau)\mathrm{d}\tau \le M_1 < \infty \tag{11}$$

where $M_1 > 0$ is a constant.

Proof: It straightforwardly follows that

$$\begin{aligned} |x| - \frac{x^2}{\sqrt{x^2 + \sigma_i^2(t)}} &\le |x| - \frac{x^2}{|x| + \sigma_i(t)} \\ &= \frac{\sigma_i(t)\,|x|}{|x| + \sigma_i(t)} < \sigma_i(t) \end{aligned} \tag{12}$$

Therefore, Eq. (8) is valid. Moreover, we can find many functions $\sigma_i(t)$ such that Eq. (9) is correct. For instance, suppose that

$$\sigma_i(t) = \exp(-a_i t) \tag{13}$$

$$\text{or} \quad \sigma_i(t) = \frac{1}{a_i t^2} \tag{14}$$

where $a_i > 0$. Then it follows that

$$\begin{aligned} \lim_{t\to\infty} \int_{t_0}^t \exp(-a_i\tau)\mathrm{d}\tau &= \lim_{t\to\infty} \frac{\exp(-a_i t_0)}{a_i} - \frac{\exp(-a_i t)}{a_i} \\ &\le \frac{\exp(-a_i t_0)}{a_i} \end{aligned} \tag{15}$$

$$\text{and} \quad \lim_{t\to\infty} \int_{t_0}^t \frac{1}{\gamma_i \tau^2}\mathrm{d}\tau = \lim_{t\to\infty} \frac{1}{\gamma_i t_0} - \frac{1}{\gamma_i t} \le \frac{1}{\gamma_i t_0} \tag{16}$$

Consequently, we can find a function such that Eq. (11) is valid.

Remark 1: Consider a function $\sigma_i(t) > 0$ that satisfis Eq. (11); then, it can be found that $\sigma_i(t) = o(1/t)$ as $t \to \infty$. Therefore, we can find that $\sigma_i(t) \to 0$ as $t \to \infty$.

Lemma 2: If the error variable $\boldsymbol{s}_i \to 0$, then $\boldsymbol{e}_{i1} \to 0$ and $\boldsymbol{e}_{i2} \to 0$ as $t \to \infty$.

Proof: Let a new variable be defined as $\boldsymbol{z}_i = \exp(k_i t)\boldsymbol{e}_{i1}$; then,

$$\dot{\boldsymbol{z}}_i = k_i \exp(k_i t)\boldsymbol{e}_{i1} + \exp(k_i t)\boldsymbol{e}_{i2} = \exp(k_i t)\boldsymbol{s}_i \tag{17}$$

It follows that

$$\boldsymbol{e}_{i1} = \exp(-k_i t)(\boldsymbol{z}_i(0) + \int_0^t \exp(k_i\tau)\boldsymbol{s}_i(\tau)\mathrm{d}\tau) \tag{18}$$

Note that

$$\forall \varepsilon > 0,\ \exists \delta_1 > 0, \forall t > \delta_1,\ \exp(k_i\tau - k_i t) < \varepsilon, \tau \in [0, t) \tag{19}$$

$$\forall \varepsilon > 0,\ \exists \delta_2 > 0, \forall t > \delta_2,\ \|\boldsymbol{s}_i(t)\| < \varepsilon \tag{20}$$

When $t > \delta_1 + \delta_2$, it is found that

$$\begin{aligned} &\left\| \int_0^t \exp(k_i\tau - k_i t)\boldsymbol{s}_i(\tau)\mathrm{d}\tau \right\| \\ &\le \|\exp(k_i\tau - k_i t)\boldsymbol{s}_i(\tau)\| + \left\| \int_{\delta_2}^t \exp(k_i\tau - k_i t)\boldsymbol{s}_i(\tau)\mathrm{d}\tau \right\| \\ &\le \varepsilon \left\| \int_0^{\delta_2} \boldsymbol{s}_i(\tau)\mathrm{d}\tau \right\| + \varepsilon \left\| \int_{\delta_2}^t \exp(k_i\tau - k_i t)\mathrm{d}\tau \right\| \\ &\le \varepsilon M_2 \end{aligned} \tag{21}$$

Consequently, $\|\boldsymbol{e}_{i1}\| \le \varepsilon z_i(0) + \varepsilon M_2$. Therefore, we can obtain that $\boldsymbol{e}_{i1} \to 0$ and $\boldsymbol{e}_{i2} = \boldsymbol{s}_i - k_i\boldsymbol{e}_{i1} \to 0$ as $t \to \infty$.

Lemma 3 [19]: For all real scalars x and all nonzero real scalars y, it follows that

$$0 \le |x| \left(1 - \tanh(|x/y|)\right) \le r\,|y| \tag{22}$$

where r is a positive constant with a minimum value of $r^* = x^*(1 - \tanh x^*)$ such that x^* satisfies $e^{-2x^*} + 1 - 2x^* = 0$.

The distributed fault-tolerant controller and adaptive laws are designed as follows:

$$\boldsymbol{f}_i = -\frac{\hat{\beta}_i^2 \boldsymbol{\xi}_i^{\mathrm{T}} \boldsymbol{\xi}_i \boldsymbol{s}_i}{\sqrt{\hat{\beta}_i^2 \boldsymbol{s}_i^{\mathrm{T}} \boldsymbol{\xi}_i^{\mathrm{T}} \boldsymbol{\xi}_i \boldsymbol{s}_i + \sigma_i^2(t)}} \tag{23}$$

$$\boldsymbol{\xi}_i = \hat{m}_i \boldsymbol{Y}_i + \lambda_i \boldsymbol{s}_i + \sum_{j=1}^n c_{ij}(\boldsymbol{s}_i - \boldsymbol{s}_j) + \hat{d}\tanh(\frac{\boldsymbol{s}_i}{\sigma_i(t)}) \tag{24}$$

$$\dot{\hat{\beta}}_i = \gamma_i \boldsymbol{s}_i^{\mathrm{T}} \boldsymbol{\xi}_i \tag{25}$$

$$\dot{\hat{m}}_i = \eta_i \boldsymbol{s}_i^{\mathrm{T}} \boldsymbol{Y}_i \tag{26}$$

$$\dot{\hat{d}}_i = -\mu_i \upsilon_i \sigma_i(t)\hat{d}_i + \mu_i \|\boldsymbol{s}_i\|_1 \tag{27}$$

where $\beta_i = \frac{1}{\alpha_i}$, $\hat{\beta}_i$ is the estimate of β_i, $\hat{m}_i$ is the estimate of the spacecraft mass m_i, $\hat{d}_i$ is the estimate of $\bar{d}_i$ such that $\hat{d}_i(0) > 0$, $\lambda_i > 0$ is a constant, c_{ij} is the element in the ith row and jth column of the adjacency matrix $\boldsymbol{C}$ of the weighted directed graph, $\sigma_i(t)$ is a bounded function that satisfies Eq. (11), and $\gamma_i > 0$, $\eta_i > 0$, $\upsilon_i > 0$, $\mu_i > 0$ are constants.

Theorem 1: For the control of the spacecraft formation system defined in Eqs. (1)-(4), if the control scheme is designed as shown in Eqs. (23)-(27), and the directed communication graph is balanced, then the position and velocity tracking errors $\boldsymbol{e}_{i1}$ and $\boldsymbol{e}_{i2}$ will converge to zero as time goes to infinity.

Proof: The following Lyapunov function candidate is selected:

$$V = \frac{1}{2}\sum_{i=1}^n m_i \boldsymbol{s}_i^{\mathrm{T}} \boldsymbol{s}_i + \sum_{i=1}^n \frac{\alpha_i}{2\gamma_i}\tilde{\beta}_i^2 + \sum_{i=1}^n \frac{1}{2\eta_i}\tilde{m}_i^2 + \sum_{i=1}^n \frac{1}{2\mu_i}\tilde{d}_i^2 \tag{28}$$

where $\tilde{\beta}_i = \hat{\beta}_i - \beta_i$, $\tilde{m}_i = \hat{m}_i - m_i$, $\tilde{d}_i = \hat{d}_i - \bar{d}_i$, and $\underline{\alpha}_i > 0$ is defined in ***Assumption 1***. It is observed that the Lyapunov function is a positive-definite function. Differentiating V yields

$$\dot{V} = \sum_{i=1}^n m_i \boldsymbol{s}_i^{\mathrm{T}} \dot{\boldsymbol{s}}_i + \sum_{i=1}^n \frac{\underline{\alpha}_i}{\gamma_i}\tilde{\beta}_i\dot{\hat{\beta}}_i + \sum_{i=1}^n \frac{1}{\eta_i}\tilde{m}_i\dot{\hat{m}}_i + \sum_{i=1}^n \frac{1}{\mu_i}\tilde{d}_i\dot{\hat{d}}_i \tag{29}$$

From Eq. (7), it follows that

$$\sum_{i=1}^n m_i \boldsymbol{s}_i^{\mathrm{T}} \dot{\boldsymbol{s}}_i = \sum_{i=1}^n \boldsymbol{s}_i^{\mathrm{T}}(m_i \boldsymbol{Y}_i + \lambda_i \boldsymbol{s}_i + \sum_{j=1}^n c_{ij}(\boldsymbol{s}_i - \boldsymbol{s}_j) + \boldsymbol{d}_i$$

$$+\boldsymbol{\Gamma}_i\boldsymbol{f}_i) - \sum_{i=1}^{n}\lambda_i\boldsymbol{s}_i^{\mathrm{T}}\boldsymbol{s}_i - \sum_{i=1}^{n}\sum_{j=1}^{n}c_{ij}\boldsymbol{s}_i^{\mathrm{T}}(\boldsymbol{s}_i-\boldsymbol{s}_j) \tag{30}$$

With the aid of ***Lemma 1*** and Eq. (23), it follows that

$$\begin{aligned}\boldsymbol{s}_i^{\mathrm{T}}\boldsymbol{\Gamma}_i\boldsymbol{f}_i &= -\frac{\hat{\beta}^2\boldsymbol{s}_i^{\mathrm{T}}\boldsymbol{\xi}_i\boldsymbol{\Gamma}_i\boldsymbol{\xi}_i^{\mathrm{T}}\boldsymbol{s}_i}{\sqrt{\hat{\beta}^2\boldsymbol{s}_i^{\mathrm{T}}\boldsymbol{\xi}_i^{\mathrm{T}}\boldsymbol{\xi}_i\boldsymbol{s}_i+\sigma_i^2(t)}}\\ &\le -\underline{\alpha}_i\frac{\hat{\beta}^2\boldsymbol{s}_i^{\mathrm{T}}\boldsymbol{\xi}_i\boldsymbol{\xi}_i^{\mathrm{T}}\boldsymbol{s}_i}{\sqrt{\hat{\beta}^2\boldsymbol{s}_i^{\mathrm{T}}\boldsymbol{\xi}_i\boldsymbol{\xi}_i^{\mathrm{T}}\boldsymbol{s}_i+\sigma_i^2(t)}}\\ &\le -\underline{\alpha}_i\hat{\beta}\boldsymbol{s}_i^{\mathrm{T}}\boldsymbol{\xi}_i+\underline{\alpha}_i\sigma_i(t)\end{aligned} \tag{31}$$

From Eq. (25), we arrive at

$$\sum_{i=1}^{n}\frac{\underline{\alpha}_i}{\gamma_i}\tilde{\beta}_i\dot{\hat{\beta}}_i = \sum_{i=1}^{n}\underline{\alpha}_i\tilde{\beta}_i\boldsymbol{s}_i^{\mathrm{T}}\boldsymbol{\xi}_i \tag{32}$$

Because the directed communication graph is balanced, $\sum_{j=1}^{n}c_{ij} = \sum_{j=1}^{n}c_{ji}$ for $i = 1, \cdots n$; thus it can be deduced that

$$\begin{aligned}&\sum_{i=1}^{n}\sum_{j=1}^{n}c_{ij}\boldsymbol{s}_i^{\mathrm{T}}(\boldsymbol{s}_i-\boldsymbol{s}_j)\\ &\quad=\sum_{i=1}^{n}\sum_{j=1}^{n}\frac{c_{ij}}{2}\boldsymbol{s}_i^{\mathrm{T}}\boldsymbol{s}_i-\sum_{i=1}^{n}\sum_{j=1}^{n}c_{ij}\boldsymbol{s}_i^{\mathrm{T}}\boldsymbol{s}_j+\sum_{j=1}^{n}\sum_{i=1}^{n}\frac{c_{ij}}{2}\boldsymbol{s}_i^{\mathrm{T}}\boldsymbol{s}_i\\ &\quad=\sum_{i=1}^{n}\sum_{j=1}^{n}\frac{c_{ij}}{2}\boldsymbol{s}_i^{\mathrm{T}}\boldsymbol{s}_i-\sum_{i=1}^{n}\sum_{j=1}^{n}\frac{c_{ij}}{2}\boldsymbol{s}_i^{\mathrm{T}}\boldsymbol{s}_j+\sum_{j=1}^{n}\sum_{i=1}^{n}\frac{c_{ji}}{2}\boldsymbol{s}_i^{\mathrm{T}}\boldsymbol{s}_i\\ &\quad=\sum_{i=1}^{n}\sum_{j=1}^{n}\frac{c_{ij}}{2}\boldsymbol{s}_i^{\mathrm{T}}\boldsymbol{s}_i-\sum_{i=1}^{n}\sum_{j=1}^{n}\frac{c_{ij}}{2}\boldsymbol{s}_i^{\mathrm{T}}\boldsymbol{s}_j+\sum_{i=1}^{n}\sum_{j=1}^{n}\frac{c_{ij}}{2}\boldsymbol{s}_j^{\mathrm{T}}\boldsymbol{s}_j\\ &\quad=\sum_{i=1}^{n}\sum_{j=1}^{n}\frac{c_{ij}}{2}(\boldsymbol{s}_i-\boldsymbol{s}_j)^{\mathrm{T}}(\boldsymbol{s}_i-\boldsymbol{s}_j)\end{aligned} \tag{33}$$

Substituting Eqs. (30)-(33) into Eq. (29), we obtain

$$\begin{aligned}\dot{V} &= \sum_{i=1}^{n}m_i\boldsymbol{s}_i^{\mathrm{T}}\dot{\boldsymbol{s}}_i+\sum_{i=1}^{n}\frac{\underline{\alpha}_i}{\gamma_i}\tilde{\beta}_i\dot{\hat{\beta}}_i+\sum_{i=1}^{n}\frac{1}{\eta_i}\tilde{m}_i\dot{\hat{m}}_i+\sum_{i=1}^{n}\frac{1}{\mu_i}\tilde{d}_i\dot{\hat{d}}_i\\ &= \sum_{i=1}^{n}\boldsymbol{s}_i^{\mathrm{T}}(m_i\boldsymbol{Y}_i+\lambda_i\boldsymbol{s}_i+\sum_{j=1}^{n}c_{ij}(\boldsymbol{s}_i-\boldsymbol{s}_j)+\boldsymbol{d}_i)+\sum_{i=1}^{n}\boldsymbol{s}_i^{\mathrm{T}}\boldsymbol{\Gamma}_i\boldsymbol{f}_i\\ &\quad+\sum_{i=1}^{n}\underline{\alpha}_i\tilde{\beta}_i\boldsymbol{s}_i^{\mathrm{T}}\boldsymbol{\xi}_i+\sum_{i=1}^{n}\frac{1}{\eta_i}\tilde{m}_i\dot{\hat{m}}_i+\sum_{i=1}^{n}\frac{1}{\mu_i}\tilde{d}_i\dot{\hat{d}}_i\\ &\quad-\sum_{i=1}^{n}\lambda_i\boldsymbol{s}_i^{\mathrm{T}}\boldsymbol{s}_i-\sum_{i=1}^{n}\sum_{j=1}^{n}c_{ij}\boldsymbol{s}_i^{\mathrm{T}}(\boldsymbol{s}_i-\boldsymbol{s}_j)\\ &\le \sum_{i=1}^{n}\boldsymbol{s}_i^{\mathrm{T}}(m_i\boldsymbol{Y}_i+\lambda_i\boldsymbol{s}_i+\sum_{j=1}^{n}c_{ij}(\boldsymbol{s}_i-\boldsymbol{s}_j)+\boldsymbol{d}_i)-\sum_{i=1}^{n}\underline{\alpha}_i\hat{\beta}\boldsymbol{s}_i^{\mathrm{T}}\boldsymbol{\xi}_i\\ &\quad+\sum_{i=1}^{n}\underline{\alpha}_i\tilde{\beta}_i\boldsymbol{s}_i^{\mathrm{T}}\boldsymbol{\xi}_i+\sum_{i=1}^{n}\frac{1}{\eta_i}\tilde{m}_i\dot{\hat{m}}_i+\sum_{i=1}^{n}\frac{1}{\mu_i}\tilde{d}_i\dot{\hat{d}}_i\end{aligned}$$

$$\begin{aligned}&-\sum_{i=1}^{n}\lambda_i\boldsymbol{s}_i^{\mathrm{T}}\boldsymbol{s}_i-\sum_{i=1}^{n}\sum_{j=1}^{n}\frac{c_{ij}}{2}(\boldsymbol{s}_i-\boldsymbol{s}_j)^{\mathrm{T}}(\boldsymbol{s}_i-\boldsymbol{s}_j)+\sum_{i=1}^{n}\underline{\alpha}_i\sigma_i(t)\\ &\le \sum_{i=1}^{n}\boldsymbol{s}_i^{\mathrm{T}}(m_i\boldsymbol{Y}_i+\lambda_i\boldsymbol{s}_i+\sum_{j=1}^{n}c_{ij}(\boldsymbol{s}_i-\boldsymbol{s}_j)+\boldsymbol{d}_i)-\sum_{i=1}^{n}\boldsymbol{s}_i^{\mathrm{T}}\boldsymbol{\xi}_i\\ &\quad+\sum_{i=1}^{n}\frac{1}{\eta_i}\tilde{m}_i\dot{\hat{m}}_i+\sum_{i=1}^{n}\frac{1}{\mu_i}\tilde{d}_i\dot{\hat{d}}_i-\sum_{i=1}^{n}\lambda_i\boldsymbol{s}_i^{\mathrm{T}}\boldsymbol{s}_i+\sum_{i=1}^{n}\underline{\alpha}_i\sigma_i(t)\\ &= \sum_{i=1}^{n}\boldsymbol{s}_i^{\mathrm{T}}(-\tilde{m}_i\boldsymbol{Y}_i-\hat{d}\tanh(\frac{\boldsymbol{s}_i}{\sigma_i(t)})+\boldsymbol{d}_i)\\ &\quad+\sum_{i=1}^{n}\frac{1}{\eta_i}\tilde{m}_i\dot{\hat{m}}_i+\sum_{i=1}^{n}\frac{1}{\mu_i}\tilde{d}_i\dot{\hat{d}}_i-\sum_{i=1}^{n}\lambda_i\boldsymbol{s}_i^{\mathrm{T}}\boldsymbol{s}_i+\sum_{i=1}^{n}\underline{\alpha}_i\sigma_i(t)\end{aligned} \tag{34}$$

From ***Lemma 3***, Eq. (22) can be rewritten as

$$-x/y\cdot\tanh(x/y) \le \alpha - |x/y| \tag{35}$$

From $\hat{d}_i(0) > 0$ and Eq. (27), we can see that $\hat{d}_i(t) > 0$ for any $t \ge 0$. Using $\hat{d}_i > 0$, $|d_{i,l}| \le \|\boldsymbol{d}_i\|_\infty \le \bar{d}_i$ and Eq. (35), we can find that

$$\begin{aligned}&\boldsymbol{s}_i^{\mathrm{T}}\boldsymbol{d}_i-\hat{d}_i\boldsymbol{s}_i^{\mathrm{T}}\tanh(\boldsymbol{s}_i/\sigma_i(t))\\ &\quad\le \|\boldsymbol{d}_i\|_\infty\|\boldsymbol{s}_i\|_1-\hat{d}_i\sigma_i(t)\cdot\boldsymbol{s}_i^{\mathrm{T}}/\sigma_i(t)\cdot\tanh(\boldsymbol{s}_i^{\mathrm{T}}/\sigma_i(t))\\ &\quad\le \bar{d}_i\|\boldsymbol{s}_i\|_1+\hat{d}_i\sigma_i(t)\sum_{l=1}^{3}-s_{i,l}/\sigma_i(t)\cdot\tanh(s_{i,l}/\sigma_i(t)))\\ &\quad\le \bar{d}_i\|\boldsymbol{s}_i\|_1+\hat{d}_i\sigma_i(t)\sum_{l=1}^{3}(\alpha-|s_{i,l}|/\sigma_i(t))\\ &\quad= \bar{d}_i\|\boldsymbol{s}_i\|_1+\hat{d}_i\sigma_i(t)(3\alpha-\|\boldsymbol{s}_i\|_1/\sigma_i(t))\\ &\quad= 3\alpha\hat{d}_i\sigma_i(t)-\tilde{d}_i\|\boldsymbol{s}_i\|_1\end{aligned} \tag{36}$$

Substituting Eqs. (26), (27) and (36) into Eq. (34), we obtain

$$\begin{aligned}\dot{V} &\le \sum_{i=1}^{n}\boldsymbol{s}_i^{\mathrm{T}}(-\tilde{m}_i\boldsymbol{Y}_i-\hat{d}\tanh(\frac{\boldsymbol{s}_i}{\sigma_i(t)})+\boldsymbol{d}_i)+\sum_{i=1}^{n}\tilde{m}_i\boldsymbol{s}_i^{\mathrm{T}}\boldsymbol{Y}_i\\ &\quad+\sum_{i=1}^{n}\tilde{d}_i\left(\|\boldsymbol{s}_i\|_1-\upsilon_i\sigma_i(t)\hat{d}_i\right)-\sum_{i=1}^{n}\lambda_i\boldsymbol{s}_i^{\mathrm{T}}\boldsymbol{s}_i+\sum_{i=1}^{n}\underline{\alpha}_i\sigma_i(t)\\ &\le -\sum_{i=1}^{n}\lambda_i\boldsymbol{s}_i^{\mathrm{T}}\boldsymbol{s}_i+\sum_{i=1}^{n}(\underline{\alpha}_i+3\alpha\hat{d}_i+\frac{\upsilon_i}{4}\bar{d}_i^2)\sigma_i(t)\end{aligned} \tag{37}$$

Integrating Eq. (37) over the interval $[0, t]$ results in

$$\begin{aligned}V(t) \le V(0)&-\sum_{i=1}^{n}\int_0^t\lambda_i\boldsymbol{s}_i^{\mathrm{T}}\boldsymbol{s}_i\mathrm{d}\tau\\ &+\sum_{i=1}^{n}\int_0^t(\underline{\alpha}_i+3\alpha\hat{d}_i+\frac{\upsilon_i}{4}\bar{d}_i^2)\sigma_i(\tau)\mathrm{d}\tau\end{aligned} \tag{38}$$

Note that $\sigma_i(\tau)$ satisfies Eq. (11), and $V(t)$ is bounded, thus $\boldsymbol{s}_i$, $\tilde{\beta}_i$, $\tilde{m}_i$, and $\tilde{d}_i$ are all bounded. From Eqs. (7), (22) and (23), it follows that

$$m_i\dot{\boldsymbol{s}}_i = m_i\boldsymbol{Y}_i+\boldsymbol{d}_i-\frac{\hat{\beta}^2\boldsymbol{\Gamma}_i\boldsymbol{\xi}_i^{\mathrm{T}}\boldsymbol{\xi}_i\boldsymbol{s}_i}{\sqrt{\hat{\beta}^2\boldsymbol{s}_i^{\mathrm{T}}\boldsymbol{\xi}_i^{\mathrm{T}}\boldsymbol{\xi}_i\boldsymbol{s}_i+\sigma_i^2(t)}} \tag{39}$$

We can find that $\dot{\boldsymbol{s}}_i$ is also bounded. From Eq. (35), we can obtain

$$\sum_{i=1}^{n}\int_0^t \lambda_i \boldsymbol{s}_i^{\mathrm{T}}\boldsymbol{s}_i \mathrm{d}\tau \le V(0) + \sum_{i=1}^{n}\int_0^t (\underline{\alpha}_i + 3\alpha\hat{d}_i + \frac{\upsilon_i}{4}\bar{d}_i^2)\sigma_i(\tau)\mathrm{d}\tau < \infty \quad (40)$$

Therefore $\boldsymbol{s}_i \in L_2$ and $\boldsymbol{s}_i \in L_\infty$. From Barbalat's Lemma [20], it can be concluded that $\boldsymbol{s}_i$ converge to zero. By virtual of ***Lemma 2***, the tracking errors $\boldsymbol{e}_{i1}$ and $\boldsymbol{e}_{i2}$ converge to zero as time goes to infinity. Because $\boldsymbol{\rho}_i - \boldsymbol{\rho}_i^{\mathrm{d}} = \boldsymbol{\rho}_i - \boldsymbol{\rho}_o^{\mathrm{d}} - \boldsymbol{\rho}_i^{\mathrm{F}}$, it is found that $\boldsymbol{\rho}_i - \boldsymbol{\rho}_i^{\mathrm{F}} \to \boldsymbol{\rho}_j - \boldsymbol{\rho}_j^{\mathrm{F}} \to \boldsymbol{\rho}_o^{\mathrm{d}}$ when $\boldsymbol{\rho}_i \to \boldsymbol{\rho}_i^{\mathrm{d}}$. Thus, the objectives of formation keeping and station keeping are realized.

Remark 2: In the proof of Theorem 1, it is assumed only that the interaction graph is balanced, which is a more general and difficult problem than those corresponding to many of the results for undirected graphs reported in [4]–[6]. Moreover, the proposed control algorithm is also valid if there is no information interaction. In such a case, the controller defined in Eqs. (23)-(27) becomes a centralized spacecraft formation tracking controller.

Remark 3: The distributed fault-tolerant controllers defined in Eqs. (23)-(27) can handle actuator faults, parameter uncertainties, and disturbances simultaneously. Adaptive laws are proposed to estimate the masses of the spacecraft, the actuator effectiveness and the upper bound on disturbances. Then, the estimated values are used in the controllers, unlike the case of the observer-based controller presented in [11]. In addition, the hyperbolic tangent function is used in the control algorithm instead of the sign function. Therefore, the undesirable chattering phenomenon will not occur.

B. ADAPTIVE CONTROLLER WITH ACTUATOR FAULTS AND COMMUNICATION DELAYS

Next, we consider time-varying coupled communication delays between the spacecraft within the formation during maneuvering. In this case, the actual information available for the ith spacecraft is the delayed information $\boldsymbol{s}_i - \boldsymbol{s}_j(t - T_{ij})$, where T_{ij} is an unknown time delay from the ith spacecraft to the jth spacecraft. A corresponding formation controller with communication delays is presented as follows:

$$\boldsymbol{f}_i = -\frac{\hat{\beta}^2\boldsymbol{\xi}_i^{\mathrm{T}}\boldsymbol{\xi}_i\boldsymbol{s}_i}{\sqrt{\hat{\beta}^2\boldsymbol{s}_i^{\mathrm{T}}\boldsymbol{\xi}_i^{\mathrm{T}}\boldsymbol{\xi}_i\boldsymbol{s}_i + \sigma_i^2(t)}} \quad (41)$$

$$\boldsymbol{\xi}_i = \hat{m}_i\boldsymbol{Y}_i + \lambda_i\boldsymbol{s}_i + \sum_{j=1}^{n} c_{ij}(\boldsymbol{s}_i - \boldsymbol{s}_j(t - T_{ij})) - \hat{d}\tanh(\frac{\boldsymbol{s}_i}{\sigma_i(t)}) \quad (42)$$

$$\dot{\hat{\boldsymbol{\beta}}}_i = \gamma_i\boldsymbol{s}_i^{\mathrm{T}}\boldsymbol{\xi}_i \quad (43)$$

$$\dot{\hat{m}}_i = \eta_i\boldsymbol{s}_i^{\mathrm{T}}\boldsymbol{Y}_i \quad (44)$$

$$\dot{\hat{d}}_i = -\mu_i\upsilon_i\sigma_i(t)\hat{d}_i + \mu_i\|\boldsymbol{s}_i\|_1 \quad (45)$$

Accordingly, the following theorem can be obtained.

Theorem 2 For the control of the spacecraft formation system defined in Eqs. (1)-(4), an adaptive fault-tolerant controller with communication delays is designed as shown in Eqs. (41)-(45). Suppose that the directed communication graph is balanced, and that the controller parameters satisfy

$$\dot{T}_{ij} \le h_{ij} < 1 \quad (46)$$

$$\lambda_i > \frac{\rho - 1}{2}\sum_{j=1}^{n} c_{ij}, \quad \rho(1 - h_{ij}) \ge 1 \quad (47)$$

for any $1 \le i, j \le n$, where $h_{ij} < 1$ is a constant, and $\rho > 1$ is a constant. Then, the position and velocity tracking errors $\boldsymbol{e}_{i1}$ and $\boldsymbol{e}_{i2}$ will converge to zero as time goes to infinity.

Proof: The following Lyapunov function candidate is selected:

$$V = \frac{1}{2}\sum_{i=1}^{n} m_i\boldsymbol{s}_i^{\mathrm{T}}\boldsymbol{s}_i + \sum_{i=1}^{n}\frac{\underline{\alpha}_i}{2\gamma_i}\tilde{\beta}_i^2 + \sum_{i=1}^{n}\frac{1}{2\eta_i}\tilde{m}_i^2 + \sum_{i=1}^{n}\frac{1}{2\mu_i}\tilde{d}_i^2 + \frac{\rho}{2}\sum_{i=1}^{n}\sum_{j=1}^{n} c_{ij}\int_{t-T_{ij}(t)}^{t}\boldsymbol{s}_j^{\mathrm{T}}(\tau)\boldsymbol{s}_j(\tau)\mathrm{d}\tau \quad (48)$$

From the proof of ***Theorem 1***, we can find that

$$\begin{aligned}\dot{V} \le & \sum_{i=1}^{n}\boldsymbol{s}_i^{\mathrm{T}}(-\tilde{m}_i\boldsymbol{Y}_i - \hat{d}\tanh(\frac{\boldsymbol{s}_i}{\sigma_i(t)}) + \boldsymbol{d}_i) \\ & - \sum_{i=1}^{n}\sum_{j=1}^{n} c_{ij}\boldsymbol{s}_i^{\mathrm{T}}(\boldsymbol{s}_i - \boldsymbol{s}_j(t - T_{ij})) \\ & + \sum_{i=1}^{n}\tilde{m}_i\boldsymbol{s}_i^{\mathrm{T}}\boldsymbol{Y}_i + \sum_{i=1}^{n}\tilde{d}_i\|\boldsymbol{s}_i\|_1 - \sum_{i=1}^{n}\lambda_i\boldsymbol{s}_i^{\mathrm{T}}\boldsymbol{s}_i + \sum_{i=1}^{n}\underline{\alpha}_i\sigma_i(t) \\ & + \frac{1}{2}\sum_{i=1}^{n}\sum_{j=1}^{n}\rho\eta_i c_{ij}(\boldsymbol{s}_j^{\mathrm{T}}\boldsymbol{s}_j - (1 - \dot{T}_{ij})\boldsymbol{s}_j^{\mathrm{T}}(t - T_{ij})\boldsymbol{s}_j(t - T_{ij}) \\ \le & -\sum_{i=1}^{n}\lambda_i\boldsymbol{s}_i^{\mathrm{T}}\boldsymbol{s}_i + \sum_{i=1}^{n}(\underline{\alpha}_i + 3\alpha\hat{d}_i)\sigma_i(t) \\ & - \sum_{i=1}^{n}\sum_{j=1}^{n} c_{ij}\boldsymbol{s}_i^{\mathrm{T}}(\boldsymbol{s}_i - \boldsymbol{s}_j(t - T_{ij})) \\ & + \frac{1}{2}\sum_{i=1}^{n}\sum_{j=1}^{n}\rho c_{ij}(\boldsymbol{s}_j^{\mathrm{T}}\boldsymbol{s}_j - (1 - \dot{T}_{ij})\boldsymbol{s}_j^{\mathrm{T}}(t - T_{ij})\boldsymbol{s}_j(t - T_{ij})\end{aligned} \quad (49)$$

Note that

$$\boldsymbol{s}_i^{\mathrm{T}}\boldsymbol{s}_j(t - T_{ij}) \le \frac{1}{2}\boldsymbol{s}_i^{\mathrm{T}}\boldsymbol{s}_i + \frac{1}{2}\boldsymbol{s}_j^{\mathrm{T}}(t - T_{ij})\boldsymbol{s}_j(t - T_{ij}) \quad (50)$$

and the directed topology is balanced, meaning that $\sum_{j=1}^{n} c_{ij} = \sum_{j=1}^{n} c_{ji}$ for $i = 1, \cdots n$; then, it follows that

$$\sum_{i=1}^{n}\sum_{j=1}^{n} a_{ij}\boldsymbol{s}_i^{\mathrm{T}}\boldsymbol{s}_i = \sum_{j=1}^{n}\sum_{i=1}^{n} a_{ji}\boldsymbol{s}_i^{\mathrm{T}}\boldsymbol{s}_i = \sum_{i=1}^{n}\sum_{j=1}^{n} a_{ij}\boldsymbol{s}_j^{\mathrm{T}}\boldsymbol{s}_j \quad (51)$$

According to Eqs. (49)-(51), the derivative of V can be rewritten as

$$\begin{aligned}\dot{V} \le & \sum_{i=1}^{n}(\underline{\alpha}_i + 3\alpha\hat{d}_i + \frac{\upsilon_i}{4}\bar{d}_i^2)\sigma_i(t) \\ & - \sum_{i=1}^{n}\sum_{j=1}^{n} c_{ij}\boldsymbol{s}_i^{\mathrm{T}}(\boldsymbol{s}_i - \boldsymbol{s}_j(t-T_{ij})) - \sum_{i=1}^{n}\lambda_i\boldsymbol{s}_i^{\mathrm{T}}\boldsymbol{s}_i \\ & + \frac{1}{2}\sum_{i=1}^{n}\sum_{j=1}^{n}\rho c_{ij}(\boldsymbol{s}_j^{\mathrm{T}}\boldsymbol{s}_j - (1-h_{ij})\boldsymbol{s}_j^{\mathrm{T}}(t-T_{ij})\boldsymbol{s}_j(t-T_{ij})) \\ \le & -\sum_{i=1}^{n}\lambda_i\boldsymbol{s}_i^{\mathrm{T}}\boldsymbol{s}_i - \sum_{i=1}^{n}\sum_{j=1}^{n} c_{ij}\boldsymbol{s}_i^{\mathrm{T}}\boldsymbol{s}_i \\ & + \sum_{i=1}^{n}(\underline{\alpha}_i + 3\alpha\hat{d}_i + \frac{\upsilon_i}{4}\bar{d}_i^2)\sigma_i(t) \\ & + \sum_{i=1}^{n}\sum_{j=1}^{n}\frac{c_{ij}}{2}(\boldsymbol{s}_i^{\mathrm{T}}\boldsymbol{s}_i + \boldsymbol{s}_j^{\mathrm{T}}(t-T_{ij})\boldsymbol{s}_j(t-T_{ij})) \\ & + \frac{1}{2}\sum_{i=1}^{n}\sum_{j=1}^{n}\rho c_{ij}(\boldsymbol{s}_j^{\mathrm{T}}\boldsymbol{s}_j - (1-h_{ij})\boldsymbol{s}_j^{\mathrm{T}}(t-T_{ij})\boldsymbol{s}_j(t-T_{ij})) \\ \le & -\sum_{i=1}^{n}(\lambda_i - \sum_{j=1}^{n}\frac{c_{ij}}{2}(\rho-1))\boldsymbol{s}_i^{\mathrm{T}}\boldsymbol{s}_i \\ & + \sum_{i=1}^{n}(\underline{\alpha}_i + 3\alpha\hat{d}_i + \frac{\upsilon_i}{4}\bar{d}_i^2)\sigma_i(t) \\ & - \sum_{i=1}^{n}\sum_{j=1}^{n}\frac{c_{ij}}{2}(\rho(1-h_{ij})-1)\,\boldsymbol{s}_j^{\mathrm{T}}(t-T_{ij})\boldsymbol{s}_j(t-T_{ij}) \quad (52)\end{aligned}$$

If Eq. (47) is satisfied, then we can obtain

$$\dot{V} \le -\sum_{i=1}^{n}\eta_i\boldsymbol{s}_i^{\mathrm{T}}\boldsymbol{s}_i + \sum_{i=1}^{n}(\underline{\alpha}_i + 3\alpha\hat{d}_i + \frac{\upsilon_i}{4}\bar{d}_i^2)\sigma_i(t) \quad (53)$$

where $\eta_i = \lambda_i - \frac{\rho-1}{2}\sum_{j=1}^{n} c_{ij} > 0$. Now we can make use of Barbalat's Lemma [20] to confirm the convergence of the position and velocity tracking errors $\boldsymbol{e}_{i1}$ and $\boldsymbol{e}_{i2}$. The derivation is similar to the proof of ***Theorem 2***; therefore, we omit it to save space.

Remark 4: Unlike the results in [16]–[18], where the constant communication delays are considered, the communication delays T_{ij} considered here are varying in time, and it is not desired that $T_{ij} = T_{ji}$ in our results. Consequently, our results are more general and extensive. However, it can be seen from Eq. (46) that the proposed control approach is applicable only to slowly-varying time delays.

IV. SIMULATION RESULTS

A. BASIC PARAMETER SETTINGS

In this section, a scenario in which four spacecraft are to perform a planned formation maneuver is considered. The directed communication topology is presented in Fig. 3, for

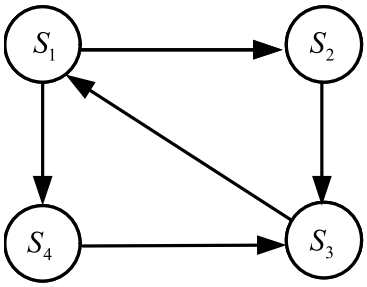

FIGURE 3. Communication topology.

which the weighted adjacency matrix is chosen to be

$$\boldsymbol{C} = [c_{ij}]_{n\times n} = \begin{bmatrix} 0 & 0 & 0.5 & 0 \\ 0.6 & 0 & 0 & 0 \\ 0 & 0.5 & 0 & 0.4 \\ 0.6 & 0 & 0 & 0 \end{bmatrix}$$

The orbital parameters of the reference spacecraft are defined as $a_c = 7000$km, $e_c = 0.02$, $\Omega_c = \pi/4$ rad, $i_c = \pi/6$ rad, $\omega_c = \pi/6$ rad, and $\theta_c(0) = 0$ rad, which is the same as [4]. The masses of the reference spacecraft is $m_c = 200$ kg. The mass of the formation spacecraft are $m_1 = 100$kg, $m_2 = 120$kg, $m_3 = 115$kg, and $m_4 = 108$kg.

The initial values of the position and velocity are given by

$$\begin{aligned}\boldsymbol{\rho}_1(0) &= [250 \;\; 20 \;\; 423]^{\mathrm{T}}\mathrm{m}, \\ \boldsymbol{\rho}_2(0) &= [-15 \;\; -505 \;\; 10]^{\mathrm{T}}\mathrm{m}, \\ \boldsymbol{\rho}_3(0) &= [-238 \;\; -10 \;\; -250\sqrt{3}]^{\mathrm{T}}\mathrm{m}, \\ \boldsymbol{\rho}_4(0) &= [5 \;\; 500 \;\; 15]^{\mathrm{T}}\mathrm{m}, \\ \boldsymbol{v}_i(0) &= [0 \;\; 0 \;\; 0]^{\mathrm{T}}\mathrm{m/s}, \quad \forall i = 1,2,3,4\end{aligned}$$

The desired positions of the spacecraft relative to the center of the formation are given by

$$\begin{aligned}\bar{\boldsymbol{\rho}}_{iF} &= R\begin{bmatrix}\frac{1}{2}\cos\varphi_i & -\sin\varphi_i & \frac{\sqrt{3}}{2}\cos\varphi_i\end{bmatrix}^{\mathrm{T}}\mathrm{m}, \\ \boldsymbol{\rho}_{iF} &= \lambda(t)\boldsymbol{R}(\bar{\varphi}(t))\bar{\boldsymbol{\rho}}_{iF}, \quad \boldsymbol{v}_{iF} = \dot{\boldsymbol{\rho}}_{iF}; \\ R &= 500\ \mathrm{m},\ \varphi_1 = 0\ \mathrm{rad},\ \varphi_2 = \frac{\pi}{2}\ \mathrm{rad},\ \varphi_3 = \pi\ \mathrm{rad}, \\ \varphi_4 &= \frac{3\pi}{2}\ \mathrm{rad}; \\ \boldsymbol{R}(\bar{\phi}(t)) &= \begin{bmatrix}\cos\bar{\phi}(t) & 0 & -\sin\bar{\phi}(t) \\ 0 & 1 & 0 \\ \sin\bar{\phi}(t) & 0 & \cos\bar{\phi}(t)\end{bmatrix}, \\ \bar{\phi}(t) &= \frac{\pi}{6}\left(1 - \exp(-0.5t^2/\chi)\right); \\ \lambda(t) &= 1 + \frac{3}{5}\left(1 - \exp(-0.5t^2/\chi)\right), \\ \chi &= -0.25T_c^2/(2\ln 10^{-6}), \quad T_c = 2\pi/n_c.\end{aligned}$$

The desired position and velocity of the center of the formation are given by

$$\boldsymbol{\rho}_o^d = \left(1 - \exp(-0.5t^2/\chi)\right)[300 \;\; 0 \;\; 0]^{\mathrm{T}}\mathrm{m}, \quad \boldsymbol{v}_o^d = \dot{\boldsymbol{\rho}}_o^d$$

In turn, the desired positions and velocities of the spacecraft within the formation are given by

$\boldsymbol{\rho}_i^d = \boldsymbol{\rho}_{iF} + \boldsymbol{\rho}_o^d, \boldsymbol{v}_i^d = \boldsymbol{v}_{iF} + \boldsymbol{v}_o^d$

The initial values of $\hat{m}_i$, $\hat{\beta}_i$, and $\hat{d}_i$ are chosen to be $\hat{m}_i(0) = 100$, $\hat{\beta}_i(0) = 1$, and $\hat{d}_i = 0.001$ $(i = 1, 2, 3, 4)$. The parameters of the controller defined in Eqs. (23)-(27) are selected to be $k_1 = 0.2$, $\lambda_i = 20$, and $\sigma_i(t) = \exp(-0.001t)$. The parameters of the controller defined in Eqs. (38)-(42) are chosen to be $k_1 = 0.2$, $\lambda_i = 15$, and $\sigma_i(t) = \exp(-0.001t)$. The communication delays for the controller defined in Eqs. (38)-(42) are set to be

$$T_{12} = 2 - \mathrm{e}^{-0.2t}\cos(0.6t), T_{13} = 1 - 0.2\cos(0.4t),$$
$$T_{14} = 1 - \mathrm{e}^{-0.5t}\sin(0.5t), T_{21} = 1 + 0.2\sin(0.2t),$$
$$T_{23} = 1 + 0.5\mathrm{e}^{-0.2t}\sin(0.4t), T_{24} = 1 + 0.4\cos(0.1t),$$
$$T_{31} = 2 + \mathrm{e}^{-0.1t}\cos(0.2t), T_{32} = 2 + 0.4\sin(0.2t),$$
$$T_{34} = 3 + 0.6\sin(0.2t), T_{41} = 1 + 0.2\cos(0.2t),$$
$$T_{42} = 2 - \mathrm{e}^{-0.4t}\cos(0.2t), \text{and} T_{43} = 1 - 0.2\cos(0.2t).$$

The components of the actuator effectiveness matrix $\boldsymbol{\Gamma}_i = \mathrm{diag}\{\alpha_{i1}, \alpha_{i2}, \alpha_{i3}\}$ are selected to be

$$\alpha_{i1}(t) = \begin{cases} 1 & t \le 10 \\ 1 - 0.1(i+1)e^{-(t-10)} & t \ge 10 \end{cases}$$
$$\alpha_{i2} = \begin{cases} 1 & t \le 15 \\ 1 - 0.1e^{-0.5i(t-15)} & t \ge 15 \end{cases}$$
$$\alpha_{i3}(t) = \begin{cases} 1 & t \le 20 \\ 1 - 0.05(i+2)e^{-0.2(t-10)} & t \ge 20 \end{cases}$$

The additive faults $\boldsymbol{\delta}_i$ are chosen such that

$$\boldsymbol{\delta}_i(t) = 0.1 \cdot \begin{bmatrix} (i+1)\cos(0.1t) + 2e^{-0.2t} \\ i\sin(0.2t) + e^{-0.3t} \\ (2i-1)\cos(0.3t) - e^{-0.4t} \end{bmatrix}^{\mathrm{T}}$$

The external disturbances are chosen such that

$$\boldsymbol{d}_i = .05 \cdot \begin{bmatrix} (i+1)\cos(0.1t) + 2i\sin(0.2t) \\ 2i\cos(0.2t) + 3i \\ (i-3)\sin(0.1t) - 2i \end{bmatrix}^{\mathrm{T}} \mathrm{N}$$

for $i = 1, 2, 3, 4$.

To quantitatively describe the formation tracking and formation keeping performance of the SFF control system, the formation tracking error μ_1 and formation keeping error μ_2 are defined as

$$\mu_1 = \frac{1}{4}\sum_{i=1}^{4} \|\boldsymbol{e}_{i1}\|_2$$
$$\mu_2 = \left|\left\|\boldsymbol{\rho}_1 - \boldsymbol{\rho}_2\right\|_2 - \left\|\boldsymbol{\rho}_1 - \boldsymbol{\rho}_3\right\|_2\right| + \left|\left\|\boldsymbol{\rho}_1 - \boldsymbol{\rho}_2\right\|_2 - \left\|\boldsymbol{\rho}_3 - \boldsymbol{\rho}_4\right\|_2\right| + \left|\left\|\boldsymbol{\rho}_2 - \boldsymbol{\rho}_4\right\|_2 - \left\|\boldsymbol{\rho}_3 - \boldsymbol{\rho}_4\right\|_2\right|$$

According to the assignment of the desired formation configuration, it can be seen that smaller μ_1 and μ_2 values during a formation maneuver indicate better performance in terms of formation tracking and formation maintenance.

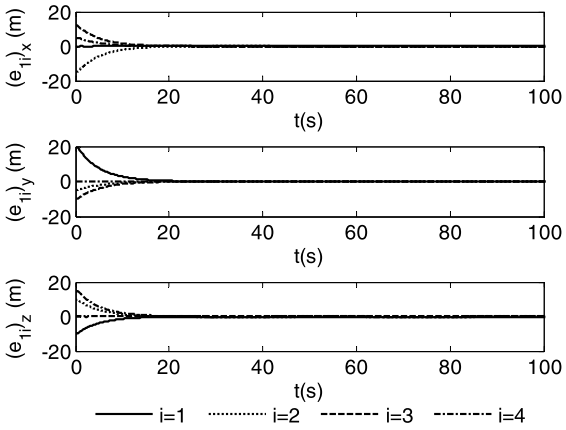

FIGURE 4. Position tracking errors with the controller defined in Eqs. (23)-(27).

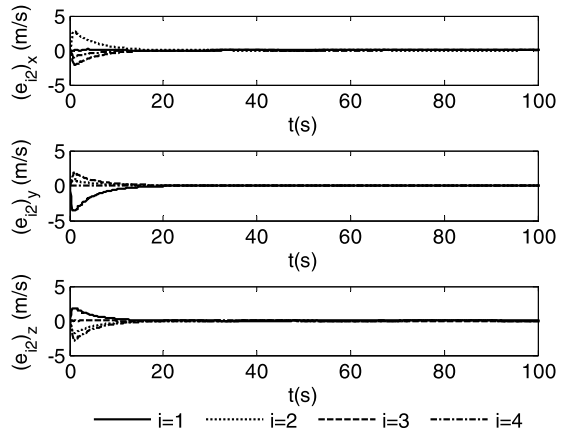

FIGURE 5. Velocity tracking errors with the controller defined in Eqs. (23)-(27).

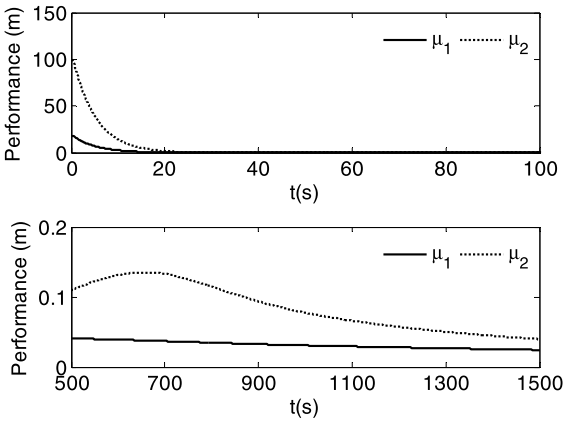

FIGURE 6. Formation tracking and keeping performance with the controller defined in Eqs. (23)-(27).

B. SIMULATION RESULTS FOR THE CONTROLLER DEFINED IN (23)-(27)

The simulation results for the controller defined in Eqs. (23)-(27) are illustrated in Fig. 4-Fig. 7. We can see from Fig. 4 that

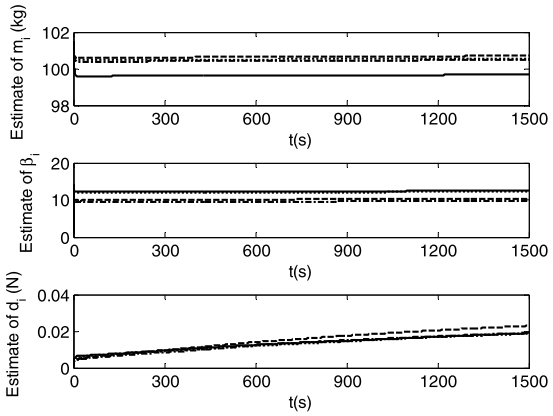

FIGURE 7. Adaptive parameters with the controller defined in Eqs. (23)-(27).

the position tracking errors $\boldsymbol{e}_{i1}$ eventually converges to zero. In addition, the spacecraft eventually reach their desired positions and follow the desired reference trajectory. The responses in terms of the velocity error $\boldsymbol{e}_{i2}$ are shown in Fig. 5. It can be observed that the velocity errors also decay quickly. Fig. 6 illustrates the formation tracking error μ_1 and the formation keeping error μ_2. The results show that μ_1 and μ_2 also converge to zero, implying favorable formation-tracking and formation-keeping performance. The responses in terms of the adaptive parameters $\hat{m}_i$, $\hat{\beta}_i$ and $\hat{d}_i$ are shown in Fig. 7, from which it can be seen that the parameters ultimately converge to constant values. Therefore the simulation results demonstrate the validity of the controllers defined in Eqs. (23)-(27) in the presence of actuator faults.

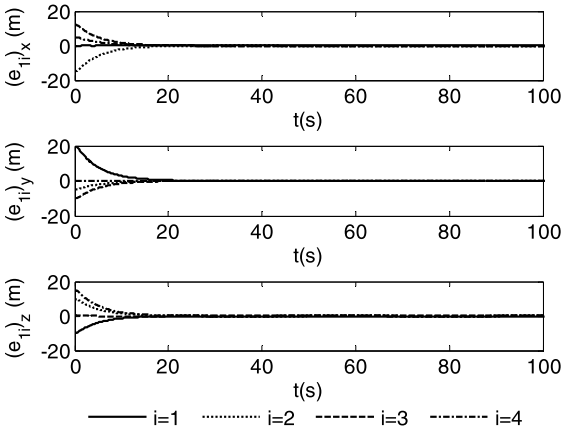

FIGURE 8. Position tracking errors with the controller defined in Eqs. (41)-(45).

C. SIMULATION RESULTS FOR THE CONTROLLER DEFINED IN (38)-(42)

The simulation results for the controller defined in Eqs. (38)-(42) are presented in Fig. 8-Fig. 11. The position tracking errors of the spacecraft are given in Fig. 8, from which it can be seen that these errors decay quickly over time. As seen

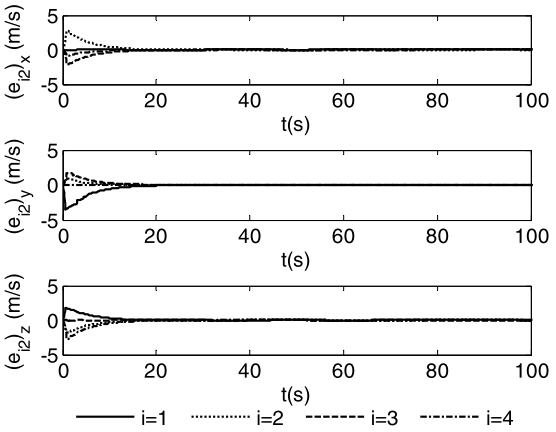

FIGURE 9. Velocity tracking errors with the controller defined in Eqs. (41)-(45).

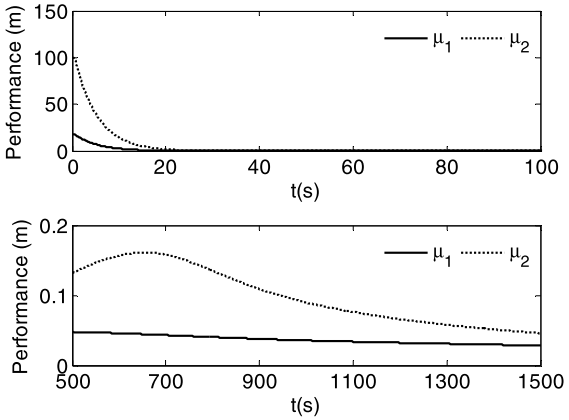

FIGURE 10. Formation tracking and keeping performance with the controller defined in Eqs. (41)-(45).

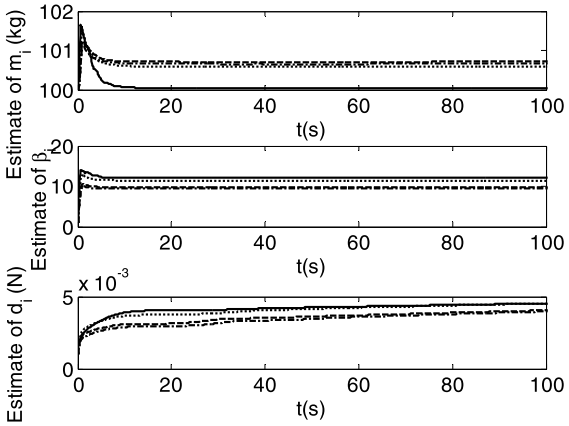

FIGURE 11. Adaptive parameters with the controller defined in Eqs. (41)-(45).

from Fig. 9, the velocity errors of the spacecraft also eventually converge to zero. Therefore, the purposes of tracking the desired trajectory and maintaining the desired configuration are fulfilled. Fig. 10 shows the responses in terms of μ_1 and μ_2 with the controller defined in Eqs. (38)-(42). It can be seen

from this figure that μ_1 and μ_2 also quickly converge to zero. The adaptive parameters $\hat{m}_i$, $\hat{\beta}_i$ and $\hat{d}_i$ are presented in Fig. 11, which shows that these parameters eventually converge to constant values. These simulations verify the feasibility of the developed control algorithms.

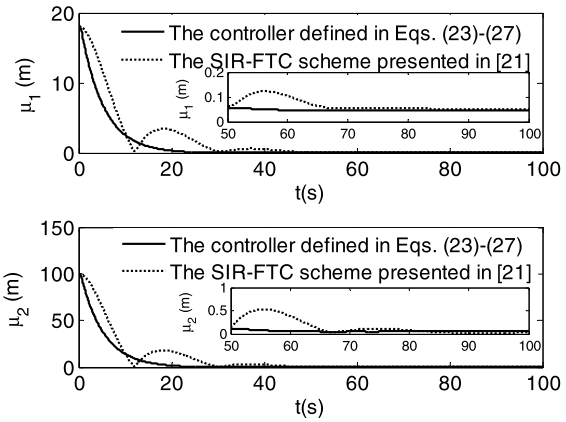

FIGURE 12. Performance with the controller defined in Eqs. (23)-(27) and the SIR-FTC scheme presented in [21].

D. THE SIMULATION COMPARISON

To illustrate the merit of the proposed control approach, a simulation comparison between the controller defined in Eqs. (23)-(27) and the SIR-FTC scheme introduced in [21] is presented. The SIR-FTC scheme can be expressed as

$$\begin{aligned} \boldsymbol{f}_i &= -(k_0 + k_i(t))\boldsymbol{s}_i \\ k_i(t) &= \frac{\hat{b}_i \Phi}{\|\boldsymbol{s}_i\| + \varepsilon} \\ \dot{\hat{b}}_i &= -\sigma_1 \hat{b}_i + \sigma_2 \frac{\|\boldsymbol{s}_i\|^2 \Phi}{\|\boldsymbol{s}_i\| + \varepsilon} \\ \varepsilon &= \frac{\mu}{1 + \Phi} \end{aligned}$$

where $k_0 > 0$, $\Phi > 0$, $\sigma_1 > 0$, $\sigma_2 > 0$, and $\mu > 0$. The parameters in the SIR-FTC scheme are chosen to be $k_0 = 20$, $\Phi = 1$, $\sigma_1 = 1$, $\sigma_2 = 10$, $\mu = 1$, and $\hat{b}_i(0) = 10$. Fig. 12 shows the responses in terms of the formation tracking error μ_1 and the formation keeping error μ_2 with the controller defined in Eqs. (23)-(27) and the SIR-FTC scheme. As seen from Fig. 12, it takes a much shorter time for the controller defined in Eqs. (23)-(27) to converge to the origin, and it does so with higher precision than the SIR-FTC scheme. Therefore, this simulation example shows the advantages of the proposed controller defined in Eqs. (23)-(27).

V. CONCLUSION

Distributed adaptive fault-tolerant coordinated control algorithms for multiple spacecraft in the presence of actuator faults, external disturbances, parameter uncertainties, and time-varying communication delays are investigated. A novel adaptive fault-tolerant controller is presented subject to unknown actuator faults, external disturbances and model uncertainties. The considered fault model allows for both additive faults and degraded actuator effectiveness. In addition, a distributed adaptive fault-tolerant controller considering time-varying communication delays is proposed. The conditions on the controller parameters and the delays that are necessary to guarantee the Lyapunov stability of the closed-loop system are given. Simulation results verify the favorable performance of the proposed control approaches. Future directions of research will include the input saturation, switching topology and collision avoidance problems. These issues will be the subject of future work.

REFERENCES

[1] S. S. Vaddi, S. R. Vadali, and K. T. Alfriend, "Formation flying: Accommodating nonlinearity and eccentricity perturbations," *J. Guid., Control, Dyn.*, vol. 26, no. 2, pp. 214–223, Mar. 2003.
[2] D. P. Scharf, F. Y. Hadaegh, and S. R. Ploen, "A survey of spacecraft formation flying guidance and control. Part II: Control," in *Proc. Amer. Contr Conf.*, Jun. 2004, pp. 2976–2985.
[3] Z. Zheng and M. Shen, "Inertial vector measurements based attitude synchronization control for multiple spacecraft formation," *Aerosp. Sci. Technol.*, vol. 93, Oct. 2019, Art. no. 105309.
[4] B.-Q. Zhang and S.-M. Song, "Decentralized coordinated control for multiple spacecraft formation maneuvers," *Acta Astronautica*, vol. 74, pp. 79–97, May 2012.
[5] K. Subbarao and S. Welsh, "Nonlinear control of motion synchronization for satellite proximity operations," *J. Guid., Control, Dyn.*, vol. 31, no. 5, pp. 1284–1294, Sep. 2008.
[6] R. Kristiansen and P. J. Nicklasson, "Spacecraft formation flying: A review and new results on state feedback control," *Acta Astronautica*, vol. 65, nos. 11–12, pp. 1537–1552, Dec. 2009.
[7] D. Ran, X. Chen, A. K. Misra, and B. Xiao, "Relative position coordinated control for spacecraft formation flying with communication delays," *Acta Astronautica*, vol. 137, pp. 302–311, Aug. 2017.
[8] Q. Hu and J. Zhang, "Relative position finite-time coordinated tracking control of spacecraft formation without velocity measurements," *ISA Trans.*, vol. 54, pp. 60–74, Jan. 2015.
[9] K. D. Kumar, "Fault tolerant reconfigurable satellite formations using adaptive variable structure techniques," *J. Guid., Control, Dyn.*, vol. 33, no. 3, pp. 969–984, May 2010.
[10] L.-B. Wu and J. H. Park, "Adaptive fault-tolerant control of uncertain switched nonaffine nonlinear systems with actuator faults and time delays," *IEEE Trans. Syst., Man, Cybern., Syst.*, early access, Feb. 11, 2019, doi: 10.1109/TSMC.2019.2894750.
[11] X. Wang and G.-H. Yang, "Fault-tolerant consensus tracking control for linear multiagent systems under switching directed network," *IEEE Trans. Cybern.*, vol. 50, no. 5, pp. 1921–1930, May 2020.
[12] Z. Gao, B. Jiang, P. Shi, M. Qian, and J. Lin, "Active fault tolerant control design for reusable launch vehicle using adaptive sliding mode technique," *J. Franklin Inst.*, vol. 349, no. 4, pp. 1543–1560, May 2012.
[13] P. Li, X. Yu, X. Peng, Z. Zheng, and Y. Zhang, "Fault-tolerant cooperative control for multiple UAVs based on sliding mode techniques," *Sci. China Inf. Sci.*, vol. 60, no. 7, Jul. 2017, Art. no. 070204.
[14] A.-M. Zou and K. D. Kumar, "Robust attitude coordination control for spacecraft formation flying under actuator failures," *J. Guid., Control, Dyn.*, vol. 35, no. 4, pp. 1247–1255, Jul. 2012.
[15] Z. Zheng, M. Qian, P. Li, and H. Yi, "Distributed adaptive control for UAV formation with input saturation and actuator fault," *IEEE Access*, vol. 7, pp. 144638–144647, 2019.
[16] A. Abdessameud, A. Tayebi, and I. G. Polushin, "Attitude synchronization of multiple rigid bodies with communication delays," *IEEE Trans. Autom., Control* vol. 57, no. 9, pp. 2405–2411, Sep. 2012.
[17] S. Li, H. Du, and P. Shi, "Distributed attitude control for multiple spacecraft with communication delays," *IEEE Trans. Aerosp. Electron. Syst.*, vol. 50, no. 3, pp. 1765–1773, Jul. 2014.
[18] M. Nazari, E. A. Butcher, T. Yucelen, and A. K. Sanyal, "Decentralized consensus control of a rigid-body spacecraft formation with communication delay," *J. Guid., Control, Dyn.*, vol. 39, no. 4, pp. 838–851, Apr. 2016.

[19] Z. Zheng and S. Song, "Cooperative attitude tracking control for multiple spacecraft using vector measurements," *Proc. Inst. Mech. Eng. G, J. Aerosp. Eng.*, vol. 229, no. 13, pp. 2375–2388, 2015.
[20] H. Khalil, *Nonlinear Systems*. 3rd ed. Upper Saddle River, NJ, USA: Prentice-Hall, 2002.
[21] W. Cai and X. H. Liao, "Indirect robust adaptive fault-tolerant control for attitude tracking of spacecraft," *J. Guid., Control, Dyn.*, vol. 31, no. 5, pp. 1456–1463, 2008.

PENG LI received the Ph.D. degree in control theory and application from the Harbin Institute of Technology, in 2010. He carried out a visiting scholar research at Wayne State University, from 2015 to 2016. He is currently an Associate Professor with the School of Automation and Electronic Information, Xiangtan University. His main research interests include robot guidance and location, and formation control.

ZONGMING LIU received the M.S. degree in control theory and application and the Ph.D. degree from the Harbin Institute of Technology, in 2011 and 2019, respectively. He is currently an Advanced Engineer with the Shanghai Institute of Spaceflight Control Technology. His main research interests include computer vision and embedded systems.

CHENYU HE received the B.S. degree in automation from the Hunan Institute of Technology, in 2018. He is currently pursuing the master's degree in control theory and control engineering with Xiangtan University, Xiangtan, China. His research interests include path optimization and multi-agent navigation.

QI LIU received the B.S. degree in electronic engineering from the Harbin University of Science and Technology, in 2018. He is currently pursuing the master's degree in control theory and control engineering with Xiangtan University. His research interests include SLAM and multi-agent navigation.

XIAO-QING LIU received the B.S. degree in automation from the Harbin University of Science and Technology, in 2005, and the M.S. degree in precision instruments and machinery from Harbin Engineering University, in 2008. She is currently pursuing the Ph.D. degree with the Department of Precision Instrument, Tsinghua University. Her current research interests include iterative learning control and integrated navigation.